CREATIVE SCIENCE

Journal home page: csj.snru.ac.th

Exploring phytochemicals and antidiabetic property of the hexane extract from *Abutilon indicum* (L.) Sweet roots

Siriporn Yaisaeng [a], Mongkol Nontakitticharoen [b], Surapon Saensouke [c], Chantana Boonyarat [d] and Siripit Pitchuanchom [a,*]

[a] *Multidisplinary Research Unit of Pure and Applied Chemistry, Department of Chemistry and Center of Excellence for Innovation in Chemistry, Faculty of Science, Mahasarakham University, Maha Sarakham, 44150, Thailand*
[b] *Natural Products Research Unit, Department of Chemistry and Center of Excellence for Innovation in Chemistry, Faculty of Science, Khon Kaen University, Khon Kaen, 40002, Thailand*
[c] *Diversity of Family Zingiberaceae and Vascular Plant for Its Applications Research Unit, Walai Rukhavej Botanical Research Institute, Mahasarakham University, Maha Sarakham, 44150, Thailand*
[d] *Division of Pharmaceutical Chemistry, Faculty of Pharmaceutical Sciences, Khon Kaen University, Khon Kaen, 40002, Thailand*

Abstract

Article history:

Received: 29-12-2025
Revised : 30-01-2026
Accepted: 02-02-2026
Published:10-02-2026

Keywords:

Abutilon indicum; Sterol; Sterol glycoside; α-glucosidase inhibitory activity; Molecular docking

The roots of *Abutilon indicum* (L.) Sweet were extracted with hexane and subjected to bioassay-guided fractionation to evaluate *α*-glucosidase inhibitory activity. The hexane extract (RAIH, 0.80% w w^{-1}) showed potent inhibition (88.06%) at 500 mg mL^{-1}. Silica gel chromatography localized the activity to fractions $RAIH_2$–$RAIH_4$ (93.55–95.19% inhibition). Chromatographic separation of the bioactive fractions afforded four known sterol-type constituents, identified by IR, ^1H NMR, and ^{13}C NMR, and compared with previously reported data as *β*-sitosterol (**1**), stigmasterol (**2**), daucosterol (**3**), and stigmasterol-3-O-*β*-D-glucoside (**4**). Compounds 3 and 4 were isolated from *A. indicum* for the first time. Although compounds **1**–4 were not assayed for *α*-glucosidase inhibitory activity in this study, literature data indicate that sterol glycosides are more potent than free sterols. Molecular docking was performed, exhibiting stronger binding for **3** and **4** than for **1** and **2**, consistent with a contributory role of sugar moieties. These findings support further compound-level validation. Therefore, investigating this plant and its chemical constituents may enhance the discovery of antidiabetic agents and related therapeutic leads. Collectively, these findings challenge the prevailing focus on polar phenolics as primary *α*-glucosidase inhibitors and highlight sterol-rich, non-polar fractions as an underexplored yet promising source of antidiabetic leads. This study provides a conceptual framework for expanding enzyme-based antidiabetic screening toward lipophilic phytochemical classes and supports further compound-level validation.

*** Corresponding author** : siripit.p@msu.ac.th
DOI: https://doi.org/10.55674/cs.v18i2.265485

1. Introduction

Postprandial hyperglycemia is increasingly recognized as a clinically important driver of type 2 diabetes (T2D) progression and a key contributor to chronic vascular complications, with postprandial glucose excursions showing strong associations with cardiovascular risk in epidemiological and mechanistic studies [1]. Therapeutically, suppression of intestinal *α*-glucosidase is an established approach for blunting postprandial glucose surges [2]. Although clinically used *α*-glucosidase inhibitors (e.g., acarbose) effectively attenuate postprandial glycemia, their frequent gastrointestinal adverse effects, such as flatulence, abdominal discomfort, and diarrhea, which are primarily attributable to colonic fermentation of unabsorbed carbohydrates, often limit long-term tolerability and adherence [3]. Moreover, the limited number of approved agents and the continued need for alternative chemotypes with improved safety profiles have sustained interest in medicinal plants and other natural sources as reservoirs of structurally diverse *α*-glucosidase inhibitors [4].

Abutilon indicum (L.) Sweet (Malvaceae), locally known in Thailand as “Ma Kong Khao” [5] (Fig. 1), is a

widely distributed shrub that thrives in disturbed and marginal habitats. The plant has a long history of use in traditional medicine. It has been associated with multiple bioactivities, including analgesic [6], antibacterial [7, 8], anti-inflammatory [9], antimycotic [10], antioxidant [8, 11], diuretic [11], antidiabetic [12], hypoglycemic [12, 13], and immunostimulant [11] effects. In addition, previous studies have reported that leaf and root extracts reduce blood glucose levels [13], with proposed mechanisms including attenuation of intestinal glucose uptake and stimulation of insulin secretion. In parallel, anti-inflammatory effects of leaf extracts have been demonstrated in experimental models, including a reduction in paw edema relative to ibuprofen [14], and antioxidant activity has been reported as comparable to reference standards.

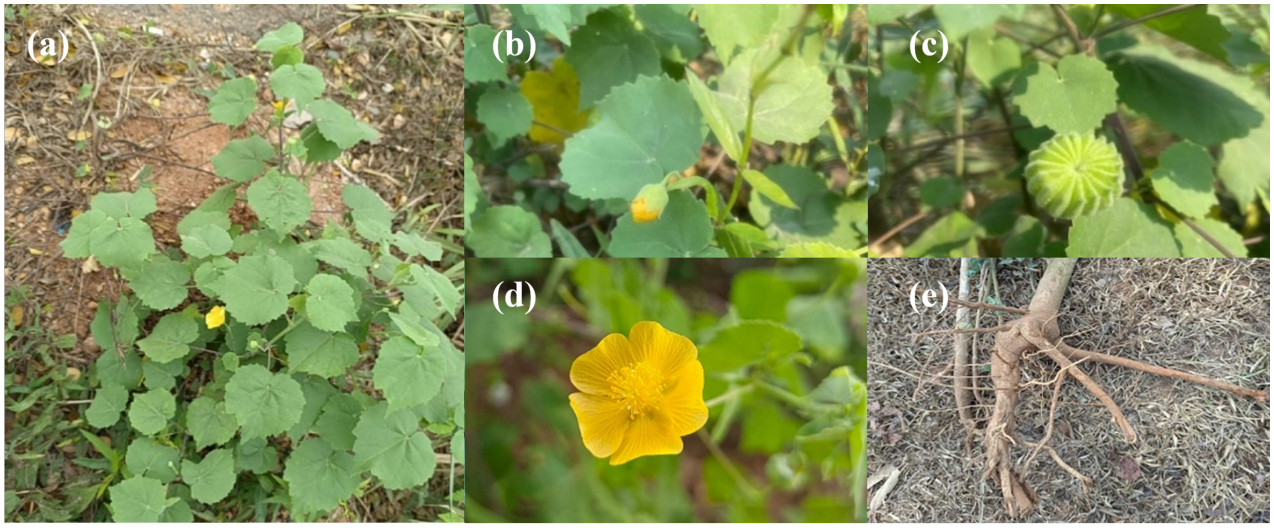

Fig. 1 The characteristics of *Abutilon indicum* (L.) Sweet collected from Mueang Khon Kaen district, Khon Kaen provice: airial part (a), leaves (b), fruit (c), flower (d), roots (e).

Phytochemical investigations have shown that *A. indicum* contains structurally diverse secondary metabolites, including flavonoids, phenolic acids, sterols, triterpenoids, alkaloids, and glycosides [15–17], which may collectively contribute to its reported bioactivities [18]. However, despite the ethnomedicinal relevance of *A. indicum* to metabolic disorders, the constituents associated with *α*-glucosidase inhibition remain insufficiently characterized, particularly in nonpolar preparations. Accordingly, the present study applied a bioassay-guided fractionation strategy to the hexane extract of *A. indicum* using silica gel column chromatography, evaluated *α*-glucosidase inhibitory activity across the crude extract and derived subfractions, and isolated four known phytosterol-type constituents, namely *β*-sitosterol (**1**), stigmasterol (**2**), daucosterol (**3**), and stigmasterol-3-O-*β*-D-glucoside (**4**) (Fig. 2).

β-Sitosterol (**1**) has been widely reported to exhibit antidiabetic, anti-inflammatory, and antioxidant activities, with evidence indicating its ability to improve glucose homeostasis, attenuate oxidative stress, and modulate metabolic signaling pathways associated with insulin sensitivity [19-21]. Stigmasterol (**2**) has similarly been shown to possess hypoglycemic and antihyperlipidemic effects, and several recent studies have demonstrated its inhibitory activity against carbohydrate-hydrolyzing enzymes, including *α*-glucosidase and *α*-amylase, thereby contributing to the regulation of postprandial hyperglycemia [22-24]. In addition, the glycosylated sterols daucosterol (**3**) and stigmasterol-3-O-*β*-D-glucoside (**4**) have been associated with a range of biological activities, including anti-inflammatory, antioxidant, and metabolic regulatory effects, as well as protective roles in models of diabetes-related complications [25-27]. The presence of a sugar moiety in these compounds has been suggested to enhance solubility and enzyme-binding interactions, and recent in vitro and in silico studies have reported antidiabetic, antihyperlipidemic, and *α*-glucosidase inhibitory properties for sterol glycosides, often exceeding those of their aglycone counterparts [28-30].

Although the purified compounds were not assayed in the present work, their reported *α*-glucosidase inhibitory activities in prior studies were used to contextualize the activity observed in the bioactive subfractions and to guide priorities for future compound-level validation.

2. Materials and Methods

General

Melting points were determined on a SANYO MPU250BM 3.5 melting point apparatus (Gallenkamp, London, UK) and uncorrected. Infrared (IR) spectra were recorded on a Bruker TENSOR 27 FTIR spectrophotometer (Bruker, Germany). The vibration bands were represented in wave number (cm^{-1}). Nuclear magnetic resonance (NMR) spectra were obtained from Bruker AVANCE NEO (400 MHz) spectrometer (Bruker, Germany). Chemical shifts were recorded on δ (ppm) scale using $CDCl_3$ and pyridine-d_5 as solvents. The internal standard was referenced from the

residual proton(s) of those deuterated solvents. ^{1}H NMR data were listed in order of the multiplicity [singlet (s), doublet (d), doublet of doublet (dd), triplet (t), and multiplet (m)] with coupling constant in Hertz, and proton position. Column chromatography (CC) was carried out over Merck silica gel (0.063–0.200 mm or less than 0.063 mm). Fractions obtained from CC were evaporated on the rotary evaporator and were analyzed by TLC on silica gel 60 F_{254} aluminium sheets. The spots were visualized under UV light at 254 and 366 nm and sprayed with anisaldehyde reagent and then heated until charred. Commercial-grade solvents were distilled at their boiling point ranges and used for extraction and chromatographic separation, whereas analytical reagent-grade solvents were used for recrystallization.

Plant material

The roots of *A. indicum* were collected in Khon Kaen Province, Thailand (GPS coordinates: 16.506° N, 102.807° E) in March 2022. The plant was identified by Assoc. Prof. Dr. Surapon Saensouk, Mahasarakham University, Thailand. The voucher specimen (No. SPMSU005) was deposited at Mahasarakham University Herbarium, Thailand.

Extraction and Isolation

The roots of *A. indicum* (6.6 kg) were air-dried, ground, and extracted at room temperature with hexane (3 × 23 L). The combined hexane extracts were concentrated under reduced pressure to afford the crude hexane extract (52.9 g; 0.80% w w^{-1}). The crude extract (52.9 g) was subjected to silica gel column chromatography (CC) and eluted with a gradient of increasing polarity using hexane, ethyl acetate (EtOAc), and methanol (MeOH). Fractions were collected and monitored by TLC, yielding seven fractions ($RAIH_1$–$RAIH_7$).

Fraction $RAIH_2$ (23.5 g) was further purified by flash column chromatography (FCC) using gradient elution of CH_2Cl_2:hexane (0:100 to 100:0, v v^{-1}), followed by MeOH:CH_2Cl_2 (0:100 to 20:80, v v^{-1}), to give 10 subfractions ($RAIH_{2.1}$–$RAIH_{2.10}$). The solid obtained from subfraction $RAIH_{2.6}$ (72 mg) was recrystallized from MeOH to afford a mixture of compounds **1** and **2** (37 mg).

Fraction $RAIH_3$ (8.2 g) was chromatographed on silica gel CC and eluted with gradient systems of CH_2Cl_2:hexane (0:100 to 100:0, v v^{-1}) and MeOH:CH_2Cl_2 (0:100 to 60:40, v v^{-1}), yielding 13 subfractions ($RAIH_{3.1}$–$RAIH_{3.13}$). Subfraction $RAIH_{3.3}$ (90 mg) was further purified on silica gel using an isocratic system of CH_2Cl_2:hexane (40:60, v v^{-1}) to yield compound **3** (46 mg).

Fraction $RAIH_4$ (5.1 g) was separated by silica gel CC using gradient elution of EtOAc:hexane (0:100 to 100:0, v v^{-1}), followed by MeOH:EtOAc (0:100 to 100:0, v v^{-1}), to afford six subfractions ($RAIH_{4.1}$–$RAIH_{4.6}$). Subfraction $RAIH_{4.6}$ was filtered, and the resulting solid was recrystallized from MeOH to provide compound **4** (0.25 g).

Compound **1** was obtained as a white solid (mixture); mp: not determined; FTIR (ATR, ν_{max} cm^{-1}): 3382, 2958, 2934, 2864, 1666, 1462, 1377, 1240, 1191, 1047, 1021, 956; ^{1}H NMR (400 MHz, $CDCl_3$, δ ppm): 5.35 (d, 1H, J = 5.7 Hz, H-6), 3.52 (m, H-3), 1.01 (d, J = 1.4 Hz, H-18), 0.92 (d, J = 6.6 Hz, H-21), 0.84 (s, H-29), 0.82 (d, J = 1.8 Hz, H-27), 0.80 (d, J = 1.8 Hz, H-26), 0.69 (s, H-19); ^{13}C NMR (100 MHz, $CDCl_3$, δ ppm): 140.74 (C-5), 121.72 (C-6), 71.81 (C-3), 56.80 (C-14), 56.04 (C-17), 51.23 (C-24), 50.13 (C-9), 42.30 (C-4), 42.20 (C-13), 40.49 (C-20), 39.76 (C-12), 37.24 (C-1), 36.13 (C-10), 33.93 (C-22), 31.89 (C-25), 31.64 (C-8), 29.13 (C-2), 29.13 (C-7), 28.24 (C-16), 26.04 (C-23), 25.40 (C-28), 24.32 (C-15), 23.05 (C-26), 21.20 (C-11), 21.07 (C-21), 19.81 (C-19), 19.02 (C-27), 12.24 (C-29), 11.97 (C-18).

Compound **2** was obtained as a white solid (mixture); mp: not determined; FTIR (ATR, ν_{max} cm^{-1}): 3382, 2958, 2934, 2864, 1666, 1462, 1377, 1240, 1191, 1047, 1021, 956; ^{1}H NMR (400 MHz, $CDCl_3$, δ ppm): 5.35 (d, J = 5.7 Hz, H-6), 5.05 (dd, J = 15.2, 8.6 Hz, H-22), 5.13 (dd, J = 15.2, 8.6 Hz, H-23), 3.52 (m, H-3), 1.01 (d, J = 1.4 Hz, H-18), 0.92 (d, J = 6.6 Hz, H-21), 0.84 (s, H-29), 0.82 (d, J = 1.8 Hz, H-27), 0.80 (d, J = 1.8 Hz, H-26), 0.69 (s, H-19); ^{13}C NMR (100 MHz, $CDCl_3$, δ ppm): 140.74 (C-5), 138.31 (C-22), 129.26 (C-23), 121.72 (C-6), 71.81 (C-3), 56.80 (C-14), 56.04 (C-17), 51.23 (C-24), 50.13 (C-9), 42.30 (C-4), 42.20 (C-13), 40.49 (C-20), 39.76 (C-12), 37.24 (C-1), 36.13 (C-10), 31.89 (C-25), 31.64 (C-8), 29.13 (C-2), 29.13 (C-7), 28.24 (C-16), 25.40 (C-28), 24.32 (C-15), 23.05 (C-26), 21.20 (C-11), 21.07 (C-21), 19.81 (C-19), 19.02 (C-27), 12.24 (C-29), 11.97 (C-18).

Compound **3** was obtained as a white solid; mp: 289–290 °C; FTIR (ATR, ν_{max} cm^{-1}): 3383, 2930, 1646, 1460, 1371, 1062; ^{1}H NMR (400 MHz, pyridine-d_5, δ ppm): 5.32 (m, H-6), 3.92 (m, H-3), 0.95 (d, J = 6.5 Hz, H-21), 0.90 (s, H-19), 0.86 (d, J = 7.2 Hz, H-26), 0.86 (t, J = 9.3 Hz, H-29), 0.84 (d, J = 7.28 Hz, H-27), 0.63 (s, H-18), 5.02 (d, J = 7.7 Hz, H-1′), 4.51 (dd, J = 11.8, 2.1 Hz, H-6′), 4.24 (m, H-3′, H-4′), 4.02 (t, J = 16.24, H-2′), 3.94 (m, H-5′); ^{13}C NMR (100 MHz, pyridine-d_5, δppm): 142.37 (C-5), 123.38 (C-6), 80.01 (C-3), 58.29 (C-17), 57.70 (C-14), 51.80 (C-9), 47.49 (C-24), 43.94 (C-13), 41.41 (C-4), 40.78 (C-12), 38.94 (C-1), 38.38 (C-10), 37.85 (C-20), 35.66 (C-22), 33.51 (C-8), 31.70 (C-7), 30.90 (C-25), 30.01 (C-2), 27.83 (C-23), 27.70 (C-28), 25.97 (C-15), 24.84 (C-16), 21.45 (C-11), 20.88 (C-27), 20.88 (C-26), 20.68 (C-21), 20.48 (C-19), 13.44 (C-18), 13.44 (C-29), 104.00 (C-1′), 79.89 (C-5′), 79.60 (C-3′), 76.75 (C-2′), 73.12 (C-4′), 64.26 (C-6′).

Compound **4** was obtained as a white solid; mp: 283–285 °C; FTIR (ATR, ν_{max} cm^{-1}): 3383, 2931, 2865, 1454, 1369, 1061; ^{1}H NMR (400 MHz, $CDCl_3$, δ ppm): 5.35 (d, J = 4.6 Hz, H-6), 5.16 (dd, J = 15.1, 8.6 Hz, H-22), 5.05 (dd, J = 15.1, 8.6 Hz, H-23), 3.14 (m, H-3), 1.00 (d, J = 6.6 Hz, H-21), 0.97 (s, H-19), 0.84 (d, J = 7.2 Hz, H-26), 0.82 (d, J = 6.8 Hz, H-27), 0.80 (t, J = 8.9 Hz, H-29), 0.67 (s, H-18), 4.88 (s(br), 1H, OH-4') 4.45 (t, J=5.8 Hz, 1H, OH-6'), 4.23 (d, J = 7.8 Hz, H-1′), 3.66 (dd, J = 6.1, 5.8 Hz, H-6′), 3.41 (m, H-3′), 3.13 (m, H-4′), 3.06 (m, H-5′), 2.19 (m, H-2′); ^{13}C NMR (100 MHz, $CDCl_3$, δ ppm): 140.08 (C-5), 138.00 (C-22), 128.63 (C-23), 121.09 (C-6), 77.75 (C-3), 56.00 (C-14),

55.41 (C-17), 49.51 (C-9), 41.65 (C-13), 39.12 (C- 12), 38.50 (C-1), 36.09 (C-10), 35.56 (C-20), 33.37 (C-2), 31.34 (C-24), 31.22 (C-25), 29.42 (C-7), 28.63 (C-8), 27.72 (C-16), 24.88 (C-15), 23.68 (C-28), 22.56 (C-11), 19.05 (C-26), 18.59 (C-19), 18.38 (C-27), 18.18 (C-21), 11.33 (C-18), 11.15 (C-29), 101.73 (C-1′), 77.63 (C-3′), 77.31 (C-5′), 74.49 (C-4′), 70.85 (C-2′), 61.98 (C-6′).

α-Glucosidase inhibitory assay

The *α*-glucosidase activity was evaluated using the modified Afrapoli's method [31]. Briefly, the enzyme solution contained 20 μL α-glucosidase (0.4 unit mL^{-1}) and 150 μL 0.08 M phosphate buffer (pH 6.9). *p*-Nitrophenyl-*α*-D-glucopyranoside (4 mM) was used as a substrate solution in the same buffer (pH 6.9). Test samples 10 μL dissolved in DMSO at various concentrations were mixed with the enzyme solution in a microplate 96 wells and incubated for 15 min at 37 °C. Acarbose was used as a positive control. Blanks were prepared by adding solvent instead of samples. Substrate solution (20 μL) was added, and the reaction was monitored by measuring absorbance at 405 nm every 2 min for 20 min. The specific activity of enzyme *α*-glucosidase was calculated as follows:

$$\text{Specific Activity } (R_s) = \frac{[\Delta OD \times \text{Volume of assay (mL)}]}{[\text{Molar absorptivity of } p\text{-NPG} \times \text{mg of protein}]}$$

Where: R_s is the rate of enzyme activity in μmole of *α*-glucosidase/minute/mg of protein; ΔOD is the change in absorbance per minute = slope; The molar absorptivity of *p*-NPG, which is 18,000 M^{-1} cm^{-1}; The enzyme inhibitory rates of each sample were calculated using the following equation:

$$\% \text{ inhibition} = \frac{(\text{control absorption} - \text{sample absorption}) \times 100}{\text{control absorption}}$$

Template Validation

The crystallographic structure of isomaltase from Saccharomyces cerevisiae, used as the *α*-glucosidase template in this study, was its complex with *α*-D-glucopyranose, a known *α*-glucosidase inhibitor. The three-dimensional coordinates were retrieved from the Protein Data Bank (PDB ID: 3A4A) [32]. To validate the docking protocol, a redocking procedure for the co-crystallized ligand was performed. Redocking results for the crystal ligand were grouped into clusters based on configurations within a 2.0 root-mean-square deviation (RMSD) tolerance of each other, obtained from 100 trials.

Molecular docking

Molecular docking was performed using AutoDock 4.2 to calculate binding free energies and determine the best orientation of all compounds with the *α*-glucosidase template. The Lamarckian Genetic Algorithm (LGA) was used for all docking calculations. Polar hydrogens and Gasteiger partial charges were assigned using AutoDockTools (ADT) in accordance with the method described by Weiner et al. [33]. Atomic solvation parameters based on the Stouten model, along with fragmental volume parameters, were incorporated into the AutoDock force field as reported by Morris et al. [34, 35]. The docking grid was centered on the co-crystallized ligand, with dimensions of 60 × 60 × 60 grid points and a grid spacing of 0.375 Å. Grid map files were generated using AutoGrid 4.2. Docking parameters included a maximum of 2.5×10^6 energy evaluations, a population size of 100 individuals, and 100 independent docking runs for each ligand. The resulting docked conformations were analyzed based on root-mean-square deviation (RMSD) from the crystal ligand, docking scores, and predicted binding free energies to elucidate interactions with the enzyme active site.

3. Results and Discussion

Structure characterization

The air-dried, powdered roots of *A. indicum* (6.6 kg) were extracted with hexane at room temperature, yielding a crude hexane extract (52.9 g) after concentration under reduced pressure. Bioassay-guided fractionation of the extract by silica gel column chromatography, followed by further chromatographic purification and recrystallization, afforded four known sterol-type constituents. Their structures were established by FTIR and NMR spectroscopic analyses and confirmed by comparison of their spectral data with those reported in the literature. The isolated compounds were identified as *β*-sitosterol (**1**), stigmasterol (**2**), and two sterol glycosides, daucosterol (**3**) and stigmasterol-3-O-*β*-D-glucoside (**4**).

Compounds **1** and **2** were obtained as a white solid mixture. The FTIR spectrum (ATR) showed a broad absorption at 3382 cm^{-1} attributable to O–H stretching, consistent with a hydroxylated sterol. Strong aliphatic C–H stretching bands at 2958, 2934, and 2864 cm^{-1} indicated a highly saturated hydrocarbon framework, while the absorption at 1666 cm^{-1} was consistent with C=C stretching of an olefinic bond. Additional bands at 1462 and 1377 cm^{-1} were assigned to aliphatic C–H bending vibrations. Prominent absorptions at 1047 and 1021 cm^{-1} further supported C–O stretching of a secondary alcohol, and the band at 956 cm^{-1} was consistent with out-of-plane deformation of an olefinic C–H, indicating a Δ^5-hydroxysterol skeleton. The ^{1}H NMR spectrum (400 MHz, $CDCl_3$) displayed a diagnostic olefinic resonance at δ_H 5.35, appearing as a doublet with a small coupling constant (J = 5.7 Hz), characteristic of the Δ^5 sterol system and corresponding to H-6 of the C-5/C-6 double bond. An oxymethine signal at δ_H 3.52 appeared as a multiplet, consistent with the C-3 proton of a 3*β*-hydroxysterol; the multiplet pattern is expected due to vicinal coupling to the neighboring C-2 and C-4 methylene protons within the rigid A-ring. The upfield region showed the typical methyl envelope of a phytosterol framework. A secondary methyl group appeared as a doublet at δ_H 0.92 (J = 6.6 Hz), indicative of coupling to an adjacent methine proton within the side chain. In contrast, additional methyl resonances were observed between δ_H 0.80–0.84. In particular,

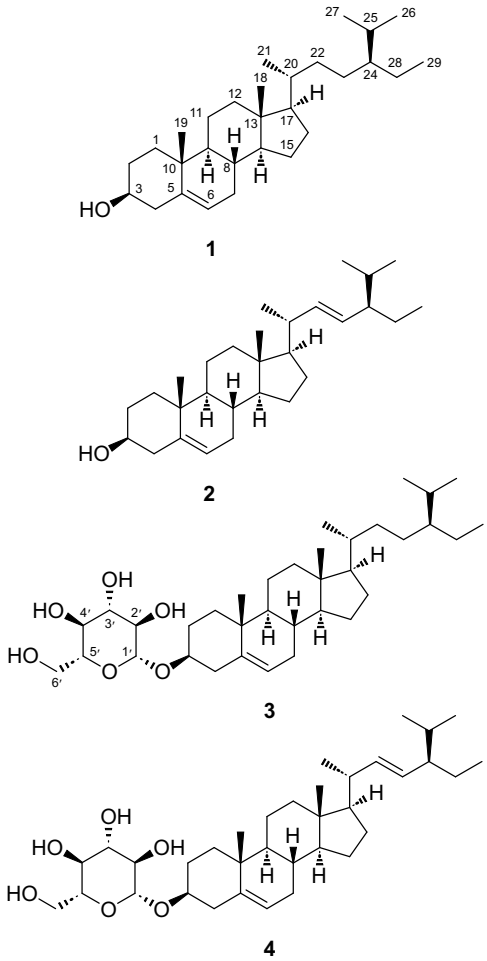

Fig. 2 Structures of the isolated compounds from the roots of *A. indicum*.

two methyl doublets at δ_H 0.82 and 0.80 are consistent with terminal side-chain methyl substituents,whereas the angular methyl group on the steroid nucleus gave a singlet at δ_H 0.69. The remaining methyl signals, including the resonance at δ_H 1.01, further supported the presence of a sitostane-type sterol component in the mixture. The ^{13}C NMR spectrum (100 MHz, $CDCl_3$) provided decisive confirmation of a Δ^5-3β-hydroxysterol framework. The presence of the C-5/C-6 double bond was supported by olefinic carbons at δ_C 140.74 (C-5) and 121.72 (C-6), while the oxygenated carbinol carbon at δ_C 71.81 (C-3) corroborated hydroxyl substitution at C-3. The remaining carbon resonances appeared in the expected aliphatic region for a phytosterol skeleton, including characteristic signals for the ring junction and side-chain carbons (e.g., δ_C 56.80, 56.04, 51.23, 50.13, and 40.49). Importantly, the side-chain positions C-22 and C-23 resonated in the saturated sp^3 region at δ_C 33.93 and 26.04, respectively, indicating the absence of an additional C-22/C-23 double bond and thereby distinguishing the sitosterol component from stigmasterol-type unsaturation. Based on the current spectral data and comparisons with those reported in the literature [24], compound **1** was identified as ***β*-sitosterol**.

In contrast, compound **2** shared the same general sterol features observed for compound **1**, as expected given that *β*-sitosterol and stigmasterol possess the same Δ^5-3*β*-hydroxysterol core. Accordingly, the FTIR profile and the major sterol signals in the ^{1}H and ^{13}C NMR spectra overlapped substantially, including the Δ^5 olefinic proton and the C-3 oxymethine resonance. The key distinction was the presence of an additional side-chain unsaturation in compound **2**. In the ^{1}H NMR spectrum, compound **2** displayed two extra downfield olefinic resonances in δ_H 5.05 (dd, J = 15.2, 8.6 Hz, H-22) and 5.13 (dd, J = 15.2, 8.6 Hz, H-23), each appearing as a doublet of doublets with a large trans-coupling constant, consistent with a trans-disubstituted C-22/C-23 double bond. This feature is absent in *β*-sitosterol and therefore serves as a clear proton-level marker to differentiate stigmasterol in the mixture. The ^{13}C NMR data provided equally definitive evidence. Whereas compound **1** exhibited saturated sp^3 carbon signals for C-22 and C-23, compound **2** showed a pronounced downfield shift for these positions into the olefinic region, with one carbon resonating at δ_C 138.31 (C-22) and the other at δ_C 129.26 (C-23), diagnostic of the C-22/C-23 double bond in stigmasterol. Thus, although both constituents share identical core sterol signatures, including C-5/C-6 and C-3, the emergence of olefinic H-22/H-23 signals in the ^{1}H NMR spectrum and the corresponding olefinic C-22/C-23 resonances in the ^{13}C NMR spectrum provide an unambiguous basis for distinguishing stigmasterol from *β*-sitosterol in the co-isolated mixture. Based on these spectral data and comparison with the reported data [36], compound 2 was identified as stigmasterol.

Compound **3** was obtained as a white solid (mp 289–290 °C). The FTIR spectrum (ATR) showed a broad O–H stretch at 3383 cm^{-1}, consistent with multiple hydroxyl groups, and a prominent aliphatic C–H stretch at 2930 cm^{-1}, supporting a highly saturated hydrocarbon framework typical of sterols. The band at 1646 cm^{-1} was attributed to C=C stretch, indicating an olefinic bond within the aglycone, whereas absorptions at 1460 and 1371 cm^{-1} corresponded to aliphatic C–H deformation. A strong absorption at 1062 cm^{-1} further supports the C–O stretch, consistent with oxygenated substituents, particularly a glycosidic linkage. The ^{1}H NMR spectrum (400 MHz, pyridine-d_5) showed resonances characteristic of a Δ^5 sterol scaffold. The vinylic proton at δ_H 5.32 (m, H-6) indicated a C-5/C-6 double bond, while the oxymethine proton at δ_H 3.92 (m, H-3) suggested oxygen substitution at C-3. The upfield region displayed a diagnostic phytosterol methyl pattern, including an angular methyl singlet at δ_H 0.63 (s, H-18) and additional methyl resonances at δ_H 0.90 (s, H-19), 0.95 (d, J = 6.5 Hz, H-21), and signals around δ_H 0.84–0.86 corresponding to side-chain methyl groups. Notably, the presence of a sugar unit was evidenced by an anomeric proton at δ_H 5.02, which appeared as a doublet (J = 7.7 Hz), diagnostic of a *β*-configured glucopyranoside. The remaining glucose proton resonances were observed in the oxygenated region, including the H-6′

oxymethylene signal at δ_H 4.51 (dd, J = 11.8, 2.1 Hz) and multiplets between δ_H 3.94–4.24 for H-2′–H-5′. The ^{13}C NMR spectrum (100 MHz, pyridine-d_5) enabled assignment of 35 carbons (with expected overlap of some methyl signals). The aglycone contained olefinic carbons at δ_C 142.37 (C-5) and 123.38 (C-6), while C-3 resonated at δ_C 80.01, consistent with glycosylation at this position. The glucose moiety was confirmed by an anomeric carbon at δ_C 104.00 (C-1′), an oxymethylene carbon at δ_C 64.26 (C-6′), and oxygenated methine carbons at δ_C 73.12–79.89 (C-2′–C-5′). These spectroscopic features are consistent with a sterol 3-O-*β*-D-glucopyranoside, and, upon comparison with previously reported data [37], compound 3 was identified as daucosterol (*β*-sitosterol-3-O-*β*-D-glucopyranoside).

Compound **4** was obtained as a white solid (mp 283–285 °C). The FTIR spectrum (ATR) exhibited a broad O–H stretching band at 3383 cm^{-1}, consistent with multiple hydroxyl groups, along with strong aliphatic C–H stretching absorptions at 2931 and 2865 cm^{-1}, supporting a sterol-type hydrocarbon framework. The absorptions at 1454 and 1369 cm^{-1} corresponded to aliphatic C–H bending vibrations. Additionally, a prominent band at 1061 cm^{-1} was assigned to C–O stretching, consistent with oxygenated functionality and a glycosidic linkage. The ^{1}H NMR spectrum (400 MHz, $CDCl_3$) displayed signals characteristic of a sterol glucoside with two sites of unsaturation. The sterol skeleton was supported by an olefinic resonance at δ_H 5.35 (d, H-6), consistent with the Δ^5 C-5/C-6 double bond, and an oxygenated methine at δ_H 3.14 (m, H-3). In addition, two further vinylic resonances at δ_H 5.16 and 5.05, each appearing as a doublet of doublets with a large trans-coupling constant (J = 15.1 Hz), were diagnostic of a trans-disubstituted side-chain double bond at C-22/C-23, a defining feature of stigmasterol-derived structures. The upfield region showed the expected methyl pattern of a phytosterol skeleton, including a secondary methyl doublet at δ_H 1.00 (J = 6.6 Hz, H-21), angular methyl singlets at δ_H 0.97 (H-19) and 0.67 (H-18), and side-chain methyl signals at δ_H 0.84, 0.82, and 0.80, consistent with the terminal methyl substituents of a stigmasterol-type aglycone. Signals attributable to the sugar moiety were clearly evident, with an anomeric proton at δ_H 4.23 appearing as a doublet with J = 7.8 Hz, indicating a *β*-configured glucopyranosyl unit. The remaining glucose protons resonated in the oxygenated region, including the H-6′ oxymethylene signal at δ_H 3.66 (dd) and multiplets corresponding to H-2′–H-5′ (δ_H 2.19–3.41). Additional downfield resonances at δ_H 4.45 and 4.88 were consistent with exchangeable hydroxyl protons. The ^{13}C NMR spectrum (100 MHz, $CDCl_3$) enabled assignment of 35 carbons, consistent with a sterol glucoside. The aglycone showed diagnostic Δ^5 olefinic carbons at δ_C 140.08 (C-5) and 121.09 (C-6), and additional olefinic carbons at δ_C 138.00 (C-22) and 128.63 (C-23), confirming the C22/C23 double bond characteristic of stigmasterol. The oxygenated C-3 carbon resonated at δ_C 77.75, consistent with glycosylation at C-3. The glucose unit was supported by an anomeric carbon at δ_C 101.73 (C-1′), an oxymethylene carbon at δ_C 61.98 (C-6′), and oxygenated methine carbons at δ_C 70.85–77.63 (C-2′–C-5′). Based on the presence of a Δ^5 sterol core, a trans C22/C23 double bond, and a *β*-D-glucopyranosyl substituent at C-3, as well as comparison of spectral data with previously reported [38], compound **4** was identified as stigmasterol-3-O-*β*-D-glucoside**.**

α-Glucosidase inhibitory activity

This study evaluated the *α*-glucosidase inhibitory activity of the crude hexane extract of *Abutilon indicum* (RAIH) and its silica gel-derived subfractions, as summarized in Table 1. At the tested concentration of 500 mg/mL, RAIH showed strong inhibition (88.06%). Bioassay-guided fractionation localized the activity to specific fractions: $RAIH_1$ remained active (75.81%), whereas $RAIH_2$–$RAIH_4$ consistently showed higher inhibition (93.55–95.19%), with $RAIH_3$ (95.19%) and $RAIH_4$ (93.81%) being the most active under these conditions. In contrast, later fractions were inactive, indicating that the inhibitory effect was confined to a defined fraction rather than broadly distributed across the extract. This activity profile guided subsequent chemical purification of the bioactive fractions and supports further compound-level evaluation to identify the constituents associated with *α*-glucosidase inhibition.

Table 1 The α-glucosidase percentage inhibitory activity of subfractions and the isolated compounds from the roots of *A. indicum*.

Fraction/Compound	% Inhibition[a]	ref
RAIH	88.06	-
$RAIH_1$	75.81	-
$RAIH_2$	93.55	-
$RAIH_3$	95.19	-
$RAIH_4$	93.81	-
$RAIH_5$	inactive	-
$RAIH_6$	inactive	-
$RAIH_7$	inactive	-
1	281.70 ± 0.24[b]	[39]
2	158.25 ± 0.90[b,c]	[40]
3	8.96 ± 0.24[b,c]	[41]
4	13.36 ± 1.17 [b,c]	[41]
Acarbose	341.14 ± 6.34[b]	-

[a]at a concentration of 500 mg mL^{-1}, [b]IC_{50} (μM), [c]Calculated from the previous reported data, inactive < 50%

Chemical investigation of the bioactive fraction space yielded four known sterol-type constituents, namely *β*-sitosterol (**1**), stigmasterol (**2**), and the sterol glycosides daucosterol (**3**) and stigmasterol-3-O-*β*-D-glucoside (**4**). Because these purified compounds were not evaluated in the present *α*-glucosidase assay, their potential contribution to the observed activity of $RAIH_2$–$RAIH_4$ can be discussed only in the context of previously reported inhibitory data. Acarbose with an IC_{50} of 341.14 μM was used as a standard reference. In the literature, *β*-sitosterol has been described as a moderate *α*-glucosidase inhibitor (reported IC_{50} 281.70 ± 0.24 μM) [39], and stigmasterol has been reported with an

IC_{50} of 158.25 ± 0.90 μM [40]. These values suggest that free phytosterols may plausibly contribute to the inhibitory profile of the lipophilic fractions, but may be insufficient to explain the near-maximal inhibition recorded for $RAIH_2$–$RAIH_4$ at the tested concentration. By contrast, sterol glycosides have been reported to exhibit substantially more potent inhibition: daucosterol has been reported with IC_{50} values of 8.96 ± 0.24 μM [41], while stigmasterol-3-O-β-D-glucoside has been reported at 13.36 ± 1.17 μM [41].

Although direct quantitative comparisons across studies are constrained by differences in enzyme source and assay format, the co-localization of strong fraction activity (RAIH2–RAIH4) with the isolation of sterols and, notably, sterol glycosides (**3** and **4**) is consistent with the rationale for a bioassay-guided approach.

Molecular docking study

To predict the interactions between compounds **1–4** and α-glucosidase, molecular docking using Autodock 4.2 was employed. Predictions in this study were based on the 3D structure of *Saccharomyces cerevisiae* α-glucosidase as a template (PDB ID 3A4A). The docking results of compounds **1**–**4** and acarbose are shown in Table 2. Sterol glycosides **3** and **4** indicated the lower binding energy better than sterols **1** and **2**, which implies that sugar moieties play a significant role in the ligand–α-glucosidase complex.

Table 2 *In silico* molecular docking results of compounds **1**–**4** with α-glucosidase.

Compound	ΔE*	K_i**
1	-9.75	71.62
2	-9.90	55.76
3	-11.81	2.20
4	-12.15	1.24
Acarbose	-8.58	517.01

*(kcal mol^{-1}), ** (nM)

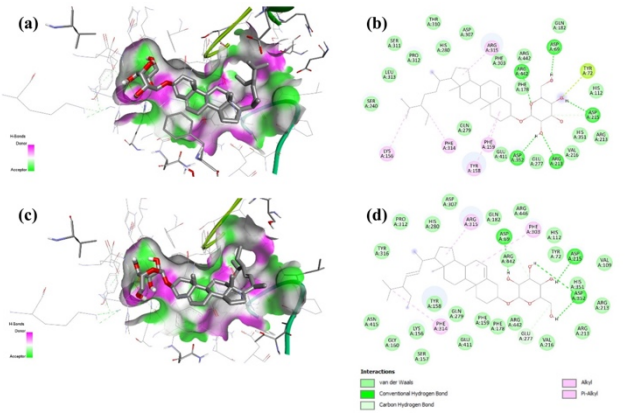

Fig. 3 Molecular docking analysis of α-glucosidase and compound **3**; 3D-diagram (a) and 2D-diagram (b) and compound **4**; 3D-diagram (c) and 2D-diagram (d).

The binding mode of compound **3** revealed that the hydroxyl groups formed four hydrogen bonds with polar residues, particularly Asp69, Asp215, Asp352, and Arg213 (Fig. 3a–b). Furthermore, the ether oxygen of the sugar ring of compound **3** formed a hydrogen bond with Phe178 as a hydrogen-bond acceptor. The residues Phe303, Asp307, His280, Pro312, Leu313, and Ser240 interact with the hydrophobic binding sites surrounding the triterpenoid region of compound **3**, which is located in the hydrophobic pocket. In addition to hydrogen bonding and general hydrophobic contacts, π–alkyl interactions play a distinct and supportive role in stabilizing the ligand–α-glucosidase complex, mediated by residues Phe159, Tyr158, Phe314, Lys156, and Arg315.

Similarly, compound **4** interacts with the enzyme α-glucosidase through hydrogen bonds, hydrophobic interactions, and π-alkyl interactions (Fig. 3c-d). The hydrogen bonds of compound **4** were formed with the Asp352, Asp215, and Arg442 residues. Hydrophobic interactions were observed between the aglycon and the amino acids His280, Pro312, Try316, Lys156, Tyr158, Gly279, and Phe159. Moreover, compound **4** also exhibited π–alkyl interactions with the Phe314, Arg315, and Phe303 residues.

The interactions between compounds **1–4** and α-glucosidase support the predicted inhibitory activity of the compounds by strengthening polar interactions mediated by noncovalent forces, thereby increasing structural stability in the active site.

4. Conclusion

Bioassay-guided fractionation of the hexane roots extract of *A. indicum* localized α-glucosidase inhibitory activity to fractions $RAIH_1$–$RAIH_4$, which showed high inhibition at 500 mg/mL. The crude hexane extract (RAIH) exhibited potent inhibition, and fractions $RAIH_2$–$RAIH_4$ consistently showed the highest effects, whereas fraction $RAIH_1$ showed moderate activity, and later fractions $RAIH_5$–$RAIH_7$ were inactive. Guided by this activity profile, silica gel column chromatography afforded four known sterol-type constituents, β-sitosterol (**1**), stigmasterol (**2**), daucosterol (**3**), and stigmasterol-3-O-β-D-glucoside (**4**). Their structures were confirmed by FTIR and NMR analyses, and by comparison of spectral data with those reported in the literature. Compounds **3** and **4** were isolated from *A. indicum* for the first time. Although compound-level α-glucosidase inhibition was not measured in this work, previously reported potencies indicate that sterol glycosides are generally more active than free sterols. A molecular docking study of compounds **1–4** against yeast α-glucosidase predicted stronger binding for **3** and **4** than for **1** and **2**, highlighting the likely contribution of sugar moieties to enzyme engagement. Collectively, these findings highlight the previously underexplored role of sterol-rich, non-polar root fractions of *A. indicum* in α-glucosidase inhibition and provide a compelling rationale for further compound-level biological validation and

mechanistic investigation aimed at developing novel antidiabetic agents.

5. Suggestions

Concentration-response testing should be performed for the crude extract (RAIH), the most active fractions (RAIH**2**–RAIH4), and the isolated constituents (**1**–**4**) under identical α-glucosidase assay conditions (enzyme source, substrate, buffer/pH, temperature, incubation time, and solvent system). In addition, enzyme kinetic analyses of the most active fractions and priority constituents, particularly sterol glycosides **3** and **4**, should be conducted to determine the mode of inhibition and support the docking-based hypotheses.

6. Acknowledgement

The authors acknowledge the Center of Excellence for Innovation in Chemistry (PERCH-CIC), Office of the Higher Education Commission, Ministry of Education, Thailand.

7. Declaration of generative AI in scientific writing

Generative AI was used solely for language editing and clarity improvements. The tool was not used to generate or modify experimental data, results, or citations. All content was carefully reviewed and approved by the authors, who take full responsibility for the final manuscript.

8. CRediT author statement

Siriporn Yaisaeng: Investigation, Formal analysis, Data curation, Visualization, Writing–Original draft.

Mongkol Nontakitticharoen: Validation, Visualization, Supervision, Writing–review & editing.

Surapon Saensouke: Resources, Supervision.

Chantana Boonyarat: Validation, Supervision.

Siripit Pitchuanchom: Funding acquisition, Project administration, Conceptualization, Methodology, Supervision, Writing – review & editing.

9. Research involving human and animals rights

Not applicable

10. Ethics Approval and Consent to Participate

Not applicable

11. Declaration of Competing Interest

The authors declare that they have no known competing financial interests or personal relationships that could have appeared to influence the work reported in this paper.

12. References

[1] Toru, H., Mutsunori, F., & Zemin Y. (2019). Postprandial hyperglycemia and postprandial hypertriglyceridemia in type 2 diabetes. *Journal of Biomedical Research*, *33*(1), 1–16. https://doi.org/10.7555/JBR.31.20160164

[2] Dirir, A. M., Daou, M., Yousef, A. F., & Yousef, L. F. (2022). A review of alpha-glucosidase inhibitors from plants as potential candidates for the treatment of type-2 diabetes. *Phytochemistry Reviews*, *21*, 1049–1079. https://doi.org/10.1007/s11101-021-09773-1

[3] Rosak, C., & Mertes, G. (2012) Critical evaluation of the role of acarbose in the treatment of diabetes: patient considerations. *Diabetes, Metabolic Syndrome and Obesity: Targets and Therapy*, *5*, 357–367. https://doi.org/10.2147/DMSO.S28340

[4] Tundis, R., Loizzo, M.R., & Menichini, F. (2010) Natural products as α-amylase and α-glucosidase inhibitors and their hypoglycaemic potential in the treatment of diabetes: an update. *Mini-Reviews in Medicinal Chemistry*, *10*, 315 – 331. https://doi.org/10.2174/138955710791331007

[5] Gamble, J. S. (2011). *Flora of the Presidency of Madras*. West, Newman and Adlard, https://doi.org/10.5962/bhl.title.21628

[6] Goyal, N., Singh, S., & Sharma, S. (2009). Analgesic effects of various extracts of the root of *Abutilon indicum* Linn. *Journal of Pharmacy and Bioallied Sciences*, *1*(1), 43. https://doi.org/10.4103/0975-7406.62686

[7] Parekh, J., & Chanda, S. (2007). Antibacterial and phytochemical studies on twelve species of Indian medicinal plants. *African Journal of Biomedical Research, 10*, 175–181.

[8] Sarkar, R., Haque, A., Ranjan, S., & Sarker, M. (2015). Phytochemical screening, antioxidant and antimicrobial effects of *Abutilon indicum* (Linn.) leaves extracts. *Pharmacologyonline, 1*, 94–103.

[9] Rajurkar, R., Jain, R., Matake, N., Aswar, P., & Khadbadi, S. S. (2009). Anti-inflammatory action of *Abutilon indicum* (L.) Sweet leaves by HRBC membrane stabilization. *Research Journal of Pharmacy and Technology, 2*(2), 415–416.

[10] Vairavasundaram, R., & Senthil, K. (2009). Antimycotic activity of the components of *Abutilon indicum* (Malvaceae). *Drug Invention Today, 1*(2), 137–139.

[11] Ramasubramania, Raja, R., & Kailasam, K. V. (2015). *butilon indicum* L. (Malvaceae): Medicinal potential review. *Pharmacognosy Journal, 7*(6), 330–332. https://doi.org/10.5530/pj.2015.6.2

[12] Krisanapun, C., Peungvicha, P., Temsiririrkkul, R., & Wongkrajang, Y. (2009). Aqueous extract of *Abutilon indicum* Sweet inhibits glucose absorption and stimulates insulin secretion in rodents. *Nutrition Research, 29*(8), 579–587. https://doi.org/10.1016/j.nutres.2009.07.006

[13] Seetharam, Y., Chalageri, G., & Ramachandra Setty, S. (2002). Hypoglycemic activity of *Abutilon indicum* leaf extracts in rats. *Fitoterapia, 73*(2), 156–159. https://doi.org/10.1016/S0367-326X(02)00015-1

[14] Tripathi, P., Chauhan, N. S., & Patel, J. R. (2012). Anti-inflammatory activity of *Abutilon indicum* extract. *Natural Product Research, 26*(17), 1659–1661. https://doi.org/10.1080/14786419.2011.616508

[15] Rajput, P., & Patel, K. (2012). Chemical investigation and biological activity of phytoconstituents from methanol extract of *Abutilon indicum* leaves. *Journal of Chemical and Pharmaceutical Research*, *4*(8), 3959–3965.

[16] Kuo, P. C., Yang, M. L., Wu, P. L., Shih, H. N., Thang, T. D., Dung, N. X., & Wub, T. S. (2008). Chemical constituents from *Abutilon indicum*. *Journal of Asian Natural Products Research*, *10*(7), 689–693.

[17] Sharma, S. K., & Goyal, N. (2010). Preliminary phytochemical and pharmacognostic profile of *Abutilon indicum* Linn. root. *Der Pharmacia Lettre*, *2*(5), 308–315.

[18] Mohite, M. S., Shelar, P. A., Raje, V. N., Babar, S. J., & Sapkal, R. K. (2012). Review on pharmacological properties of *Abutilon indicum*. *Asian Journal of Pharmaceutical Research*, *2*(4), 156–160.

[19] Adhimoolam, K., Sureshbabu, A., Smirnova, E., Muthuramalingam, P., Thi, C. T. D., Senthil, K., & Min, T. (2024). β-Sitosterol–Dietary sources and role in cancer and diabetes management. *Food Science & Nutrition*, *12*(11), 8870–8886. http://doi:10.1002/fsn3.4380

[20] Durrani, A. K., Khalid, M., Raza, A., Rasool, I. F.U., Khalid, W., Akhtar, M. N., Khan, A. A., Abdullah, Z., & Khadijah, B. (2024). Clinical improvement, toxicity and future prospects of β-sitosterol: a review. *CyTA – Journal of Food, 22*(1), 2337886. https://doi.org/10.1080/19476337.2024.2337886

[21] Zhang, D., Ge, F., Ji, J., Li, Y. J., Zhang, F. R., Wang, S. Y., Zhang, S. J., Zhang, D. M., & Chen, M. (2023). β-sitosterol alleviates dextran sulfate sodium-induced experimental colitis via inhibition of NLRP3/Caspase-1/GSDMD-mediated pyroptosis. *Frontiers in Pharmacology, 14*, 1218477. https://doi:10.3389/fphar.2023.1218477

[22] Poulose, N., Sajayan, A., Ravindran, A., Chandran, A., Priyadharshini, G. B., Selvin, J., & Kiran, G. S. (2021). Anti-diabetic potential of a stigmasterol from the seaweed *Gelidium spinosum* and its application in the formulation of nanoemulsion conjugate for the development of functional biscuits. *Frontiers in Nutrition, 16*(8), 694362. https://doi: 10.3389/fnut.2021.694362

[23] Li, J., Zheng, X., & Qi, J. (2025). Research progress on the therapeutic mechanisms of stigmasterol for multiple diseases. *Molecules, 30*(9), 1874. https://doi: 10.3390/molecules30091874

[24] Miya, G. M., Kar, P., Oriola, A. O., & Oyedeji, A. O. (2025). Antidiabetic potential of isolated compounds from *Cyperus sexangularis* Nees: An in silico molecular docking and dynamic-based approach. *Journal of Pharmacy & Pharmacognosy Research, 13*(2), 647–661. https://doi.org/10.56499/jppres24.2050_13.2.647

[25] Liang, J., Yang, H., Chen, K., Cai, J., Wang, Y., & Yong, Y. (2025). Therapeutic effect of daucosterol on DSS-induced colitis in mice. *BMC Microbiology*, *4*(26), 18. https://doi: 10.1186/s12866-025-04556-6

[26] Omari, N. E., Jaouadi, I., Lahyaoui, M., Benali, T., Taha, D., Bakrim, S., Menyiy, N. E., Kamari, F. E., Zengin, G., Bangar S. P., Lorenzo, J. M., Gallo, M., Montesano, D., & Bouyahya, A. (2022). Natural sources, pharmacological properties, and health benefits of daucosterol: versatility of actions. *Applied Sciences, 12*, 5779. https://doi.org/10.3390/app12125779

[27] Mohammed, I. H., Zarial, V., Farimani, M. M., Kharatha, M., Tabefam, M., & Kakey, E. S. I. (2025). In vitro assessment of the antihyperglycemic property of *Prosopis farcta* J. F. Macbr and *Rheum ribes* L. and phytochemical profiling of the most active extract. *Trends in Phytochemical Research, 9*(2), 092511. https://doi.org/10.57647/tpr.2025.0902.11

[28] Pate, A. K., & Kayande, N. R. (2023). An insilico study of stigmasterol glucoside for hypolipidemic activity. *Biological Forum – An International Journal, 15*(4), 660–667.

[29] Ditchou, Y. O. N., Leutcha, P. B., Miaffo, D., Mamoudou, H., Ali, M. S., Ngnoung, G. A. A., Soh, D., Agrawal, M., Darbawa, R., Tchouboun, E. Z. N., Lannang, A. M., & Noundou, X. S. (2024). In vitro and in silico assessment of antidiabetic and antioxidant potencies of secondary metabolites from *Gymnema sylvestre. Biomedicine&Pharmacotherapy, 177*, 117043. https://doi.org/10.1016/j.biopha.2024.117043

[30] Zaid, O. A. A., Moawed, F. S. M., Ismail, E. S., & Farrag, M. A. (2023). β-sitosterol attenuates high- fat diet-induced hepatic steatosis in rats by modulating lipid metabolism, inflammation and ER stress pathway. *BMC Pharmacology and Toxicology, 24*, 31. https://doi.org/10.1186/s40360-023-00671-0

[31] Moradi-Afrapoli, F., Asghari, B., Saeidnia, S., Ajani, Y., Mirjani, M., Malmir, M., Bazaz, R. D., Hadjiakhoondi, A., Salehi, P., Hamburger, M., & Yassa, N. (2012). In vitro *α*-glucosidase inhibitory activity of phenolic constituents from aerial parts of *Polygonum hyrcanicum*. *DARU Journal of Pharmaceutical Sciences, 20*, 37. https://doi.org/10.1186/2008-2231-20-37

[32] Yamamoto, K., Miyake, H., Kusunoki, M., & Osaki, S. (2010). Crystal structures of isomaltase from *Saccharomyces cerevisiae* and in complex with its competitive inhibitor maltose. *FEBS Journal*, *277*, 4205–4214.

[33] Weiner, S. J., Kollman, P. A., Case, D. A., Singh, U. C., Ghio, C., Alahona, G., Profeta, S., & Weiner, P. (1984). A new force field for molecular mechanical simulation of nucleic acids and proteins. *Journal of the American Chemical Society, 106*, 765–784.

[34] Morris, G. M., Goodsell, D. S., Halliday, R. S., Huey, R., Hart, W. E., Belew, R. K., & Olson, A. J. (1998). Automated docking using a lamarckian genetic algorithm and an empirical binding free energy function. *Journal of Computational Chemistry*, *19*, 1639–1662.

[35] Yamamoto, K., Miyake, H., Kusunoki, M., & Osaki, S. (2010). Crystal structures of isomaltase from *Saccharomyces cerevisiae* and in complex with its competitive inhibitor maltose. *FEBS Journal*, *277*, 4205–4214.

[36] Chaturvedula, V. S. P., & Prakash, I. (2012). Isolation of Stigmasterol and B -sitosterol from the dichlomethane extract of *Rubus suavissmus*. *International Current Pharmaceutical Journal*, *1*(9):239–242.

[37] Esmaeili, M. A., & Farimani, M. M. (2014). Inactivation of PI3K/Akt pathway and upregulation of PTEN gene are involved in daucosterol-induced apoptosis in human breast adenocarcinoma cells. *South African Journal of Botany, 93*, 37–47. https://doi.org/10.1016/j.sajb.2014.03.010

[38] Afrizal, S., & Mai, E. (2015). Isolation and elucidation structure of stigmasterol glycoside from *Nothopanax scutellarium* Merr leaves. *Journal of Chemical and Pharmaceutical Research, 7*(12), 763–765.

[39] Tabussum, A., Riaz, N., Saleem, M., Ashraf, M., Ahmad, M., Alam, U., Jabeen, B., Malik, A., & Jabbar, A. (2013). *α*-Glucosidase inhibitory constituents from *Chrozophora plicata*. *Phytochemistry Letters*, *6*(4), 614–619 http://doi.org/10.1016/j.phytol.2013.08.005

[40] Murugesu, S., Ibrahim, Z., Ahmed, Q. U., Yusoff, N. I. N., Uzir B. F., Perumal, V., Abas, F., Saari, K., Hesham, E. S., & Khatib, A. (2018). Characterization of α-glucosidase inhibitors from *Clinacanthus nutans* Lindau leaves by Gas Chromatography-Mass Spectrometry-Based metabolomics and molecular docking simulation. *Molecules*, *23*, 2402. http://doi.org/10.3390/molecules23092402

[41] Gu, Y., Yang, X., Shang, C., Thao, T. T. P., & Koyama, T. (2021). Inhibitory properties of saponin from *Eleocharis dulcis* peel against *α*-glucosidase. *RSC Advances*, *11*, 15400–15409. http://doi.org/10.1039/d1ra02198b